Available online at www.sciencedirect.com
SCIENCE DIRECT®
Journal of Power Sources 138 (2004) 41–50
JOURNAL OF POWER SOURCES
www.elsevier.com/locate/jpowsour

Oxygen mass transfer in PEM fuel cell gas diffusion layers

K.T. Jeng*, S.F. Lee, G.F. Tsai, C.H. Wang

Department of Mechanical and Automation Engineering, Dayeh University, Chang-Hwa 515-05, Taiwan

Received 16 February 2004; received in revised form 11 June 2004; accepted 14 June 2004
Available online 5 August 2004

Abstract

A simple two-dimensional model involving kinetics and mass transfer in a PEM fuel cell cathode is presented. In this model, the catalyst layer was simplified as an infinite thin film. The oxygen mass transfer in the gas diffusion layer (GDL) was described using a pure diffusion equation that introduced equivalent oxygen diffusivity. The PEM fuel cell performance under the influence of current collector ribs was investigated. The results show that, the existence of ribs causes the GDL to be used only partly in the mass transfer process. The GDL effectiveness decreases with the cell current density and increases with the width of the gas flow channels. The PEM fuel cell performance decreases with an increase in GDL thickness if the GDL porosity is low. However, when a high-porosity GDL is used, the optimal thickness becomes an indicator determining the maximal PEM fuel cell performance.

Keywords: PEMFC; Fuel cell; Gas diffusion layer; Mass transfer

1. Introduction

Most PEM fuel cell designs are based on planar and repetitively stacked structures. Each cell in the stack has two bipolar plates pressed against the membrane electrode assembly (MEA), as shown in Fig. 1. The MEA is the core component of PEM fuel cells, which consists of the proton exchange membrane (PEM), anode and cathode electrodes. An electrode comprises both the gas diffusion layer (GDL) and the catalyst layer. The GDL is usually made of carbon papers or carbon cloths, forming the outmost portion of the MEA and positioned next to the bipolar plate. The gas flow channels grooved on both sides of the bipolar plate are designed to distribute the reactant gas to the electrode reaction sites. The current collector ribs laid between two neighbouring channels are the paths for the electric current.

Because the electrode portion covered by the ribs is not directly exposed to the channels, it suffers from a slow reactant gas mass transfer. The ribs can be regarded as barriers to mass transfer; however, they are indispensable to electric current conduction in a PEM fuel cell.

A complete understanding of the mass transfer phenomena within the GDL, under the influence of current collector ribs, will facilitate a proper PEM fuel cell design. However, there have been very few studies in the literature dealing with such a critical problem. West and Fuller [1] studied the effects of rib sizing and the GDL thickness on the current and water distributions within a PEM fuel cell. They found that the ribs only slightly altered the cathode potential for a given current density, but had a significant influence on water management. Hental et al. [2] experimentally investigated the effects of both rib and channel widths on the performance of single PEM fuel cells. Recently, Yan et al. [3] developed a two-dimensional mass transport model to investigate the anode gas flow channel cross section and GDL porosity effects. They found that an increase in either the GDL porosity, channel width fraction, or the number of channels could lead to better cell performance.

The PEM fuel cell anode overpotential is negligible in comparison with the cathode overpotential, thus the hydrogen mass transport at the anode is considered less significant than the oxygen mass transport at the cathode. The purpose of

* Corresponding author. Tel.: +886 4 851 1224; fax: +886 4 851 1224.
E-mail address: jeng@mail.dyu.edu.tw (K.T. Jeng).

0378-7753/$ – see front matter © 2004 Elsevier B.V. All rights reserved.
doi:10.1016/j.jpowsour.2004.06.019

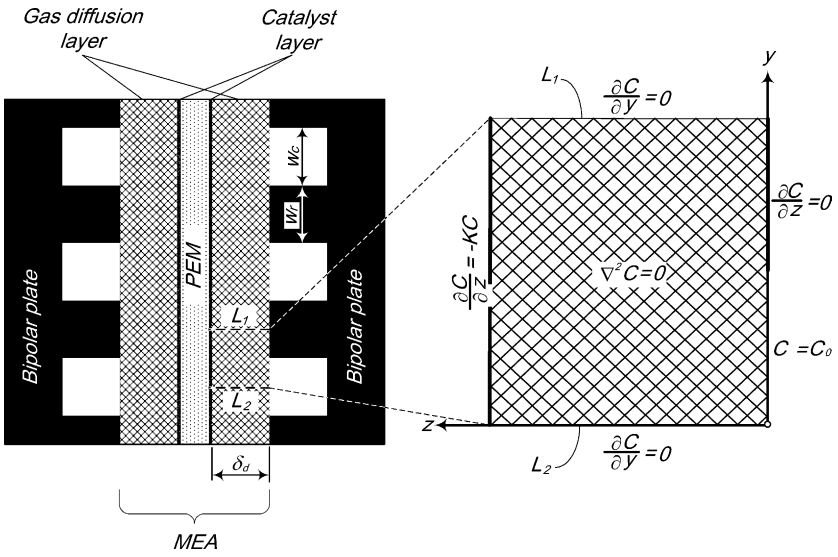

Fig. 1. Schematic diagram of the PEM fuel cell and the enlarged gas diffusion layer element.

this study is to investigate the effect of current collector ribs on the oxygen mass transfer through the GDL. We will determine the equivalent oxygen diffusivity within the GDL in an operating PEM fuel cell using a one-dimensional model first. The so obtained equivalent diffusivity will then be used to describe the oxygen mass transfer in the cathode gas mixture under the influence of ribs using a two-dimensional model. Figures on the distribution of oxygen concentration within the GDL and the variation in current density along the catalyst layer will be recorded. The rib effects on the cell performance and on the GDL effectiveness are to be investigated. This study provides a novel method in enhancing the oxygen mass transfer through the GDL.

2. Equivalent oxygen diffusivity in cathode gas mixture

In this study, a two-dimensional model for oxygen mass transport within a GDL has been simplified into a pure diffusion problem by the introduction of an equivalent oxygen diffusivity. To obtain the equivalent oxygen diffusivity, the mass transfer within the GDL is investigated using a one-dimensional model as the starting point.

2.1. One-dimensional model

The one-dimensional GDL model is schematically shown in Fig. 2. Let $z = 0$ specify the GDL/channel interface and z increase in the oxygen transport direction. The gas phase in the GDL is a mixture of oxygen, water vapour and nitrogen (if air is used as the cathode gas). We assume that the cathode gas mixture acts as an ideal gas and the fuel cell operates under steady-state conditions. The Stefan–Maxwell equation for multi-component diffusion can be used to describe the gradient in the component mole fractions:

$$\frac{\mathrm{d}x_i}{\mathrm{d}z} = \sum \frac{RT}{P_t D_{ij}^{\mathrm{eff}}}(x_i N_j - x_j N_i) \tag{1}$$

where x_i and N_i represent, respectively, the mole fraction and the molar flow rate of species i. D_{ij}^{eff}, the effective binary diffusivity of the gas pair i–j in the porous media, and P_t, the pressure of the gas mixture in the GDL which is considered to be constant and equal to that in the gas flow channel. The effective binary diffusivity can be evaluated from the bulk binary diffusivity D_{ij} using Bruggeman's correction [4]:

$$D_{ij}^{\mathrm{eff}} = \varepsilon^{3/2} D_{ij} \tag{2}$$

where ε is the porosity of the GDL.

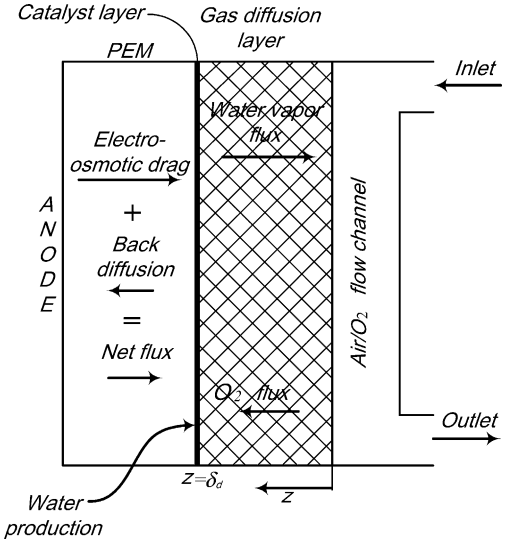

Fig. 2. Schematic diagram of the one-dimensional model.

Under steady-state conditions and from species conservation, we have observed that the molar flow rates of the oxygen, water vapor and nitrogen are all constant. Discounting the crossover of the reactant gases, the oxygen molar flow rate can be related to the current density I as:

$$N_{\mathrm{o}} = \frac{I}{4F} \tag{3}$$

Because nitrogen is inert, we have:

$$N_{\mathrm{n}} = 0 \tag{4}$$

The water vapor transport rate through the GDL is the sum of the water production rate at the catalyst layer, $I/2F$, and the water transport rate through the PEM, which is equal to the water flow rate dragged by protons (electro-osmotic drag) minus the water back diffusion rate due to the water concentration gradient in the PEM.

2.2. Net electro-osmotic drag coefficient

A net electro-osmotic drag coefficient β is defined as the number of net water molecules transported from the anode to the cathode per proton [5]. This can be used to relate the net water flow rate through the PEM with the current density I. Assuming that, within the GDL, the water vapor is transported in a direction opposite to z, the flow rate of the water vapor takes the form of:

$$N_{\mathrm{w}} = -\left(\beta + \frac{1}{2}\right)\frac{I}{F} \tag{5}$$

The net water flow rate through the PEM has been investigated by using model simulations [5,6] or experimental methods [7,8]. It has been found that β is determined by the operating conditions (such as, current density, temperature, pressure, stoichiometry and humidity of the inlet gases), and the membrane thickness. Choi et al. [7] reported that the value of β decreases with the current density, but it is nearly constant above a current density of 200 mA cm^{-2}. For Nafion® 115, the constant is around 0.3 under operating conditions of 70 °C, 1 atm H_2/O_2, and humidified reactant gases. The constant goes up to 0.4 when the O_2 is not humidified. Janssen and Overvelde [8] reported that, for Nafion® 105, the constant is around 0.2 under operating conditions of 80 °C, 1.5 atm H_2/air, and humidified H_2. The β value has been set to 0.35 when we calculate the equivalent oxygen diffusivity in the cathode gas mixture.

Combining Eqs. (3)–(5) with Eq. (1), one can obtain the following two differential equations for x_{o} and x_{n}:

$$\frac{P_t}{RT}\frac{\mathrm{d}x_{\mathrm{o}}}{\mathrm{d}z} = -\left[\frac{x_{\mathrm{o}}}{D^{\mathrm{eff}}_{\mathrm{w-o}}}(4\beta+2) + \left(\frac{x_{\mathrm{w}}}{D^{\mathrm{eff}}_{\mathrm{w-o}}} + \frac{x_{\mathrm{n}}}{D^{\mathrm{eff}}_{\mathrm{n-o}}}\right)\right]\frac{I}{4F} \tag{6}$$

$$\frac{P_t}{RT}\frac{\mathrm{d}x_{\mathrm{n}}}{\mathrm{d}z} = \left[\frac{-1}{D^{\mathrm{eff}}_{\mathrm{w-n}}}(4\beta+2) + \frac{1}{D^{\mathrm{eff}}_{\mathrm{n-o}}}\right]\frac{x_{\mathrm{n}} I}{4F} \tag{7}$$

Because the cathode gas mixture consists of oxygen, water vapor, and nitrogen, the following relation for the mole fraction holds:

$$x_{\mathrm{o}} + x_{\mathrm{w}} + x_{\mathrm{n}} = 1 \tag{8}$$

Both Eqs. (6) and (7) can be integrated along with Eq. (8), from the initial $x_{\mathrm{o}}|_{z=0}$, $x_{\mathrm{w}}|_{z=0}$, and $x_{\mathrm{n}}|_{z=0}$ values, to yield the spatial variation in x_{o}, x_{w} and x_{n} throughout the GDL. The $x_{\mathrm{o}}|_{z=0}$ and $x_{\mathrm{n}}|_{z=0}$ values can easily be evaluated as long as the $x_{\mathrm{w}}|_{z=0}$ value is set.

When solving Eqs. (6)–(8), we assume that the water vapor is saturated at the GDL/catalyst layer interface. Thus, the chosen $x_{\mathrm{w}}|_{z=0}$ value must make the partial pressure of water vapor at $z = \delta_{\mathrm{d}}$ satisfy the following relation:

$$x_{\mathrm{w}}|_{z=\delta_{\mathrm{d}}} P_t = P^{\mathrm{sat}}_{\mathrm{w}} \tag{9}$$

where $P^{\mathrm{sat}}_{\mathrm{w}}$ denotes the saturation pressure of water vapor at the PEM fuel cell operating temperature. This consequently results in a shooting problem in terms of the initial $x_{\mathrm{w}}|_{z=0}$ value, which can be solved using the appropriate shooting technique [9].

Fig. 3 shows the x_{o}, x_{w} and x_{n} profiles in the one-dimensional GDL for three different current densities when air at 1 atm is supplied to the cathode channel. The estimated parameters and properties used to describe the GDL one-dimensional mass transfer are given in Table 1. As can be seen from Fig. 3, all of the mole fraction graphs are almost linear within the GDL for the current densities investigated. Other results (not shown here) indicate that the linearity holds up to a GDL thickness greater than 1 mm and higher porosity dose not break the linearity either. The reason why there is a linear variation in the mole fractions is because the GDL thickness is very small. The linearity of the graphs suggests an "equivalent diffusivity" approach to resolving the GDL mass transfer problem.

2.3. Equivalent oxygen diffusivity estimation

Fick's law in terms of the molar flow rate of oxygen, as shown below, can be used to describe the transport of oxygen in the GDL:

$$N_{\mathrm{o}} = x_{\mathrm{o}} \sum_{j=\mathrm{o,n,w}} N_j - (\varepsilon^{3/2} D_{\mathrm{o\text{-}mix}})\frac{\mathrm{d}C}{\mathrm{d}z} \tag{10}$$

Table 1
Physical parameter and property values used in one-dimensional model

Physical parameter/property	Value
Cell temperature, T (K)	353.15
Thickness of gas diffusion layer, δ_{d} (cm)	0.03
Gas-pair pressure-diffusivity product, $P_t D_{\mathrm{n-o}}$ (atm cm^2 s^{-1})	0.279 [10]
Gas-pair pressure-diffusivity product, $P_t D_{\mathrm{w-o}}$ (atm cm^2 s^{-1})	0.37 [10]
Gas-pair pressure-diffusivity product, $P_t D_{\mathrm{w-n}}$ (atm cm^2 s^{-1})	0.387 [10]
Net electro-osmotic drag coefficient, β	0.35
Porosity of gas diffusion layer, ε	0. 3
Nitrogen–oxygen mole ratio in gas flow channel	3.76

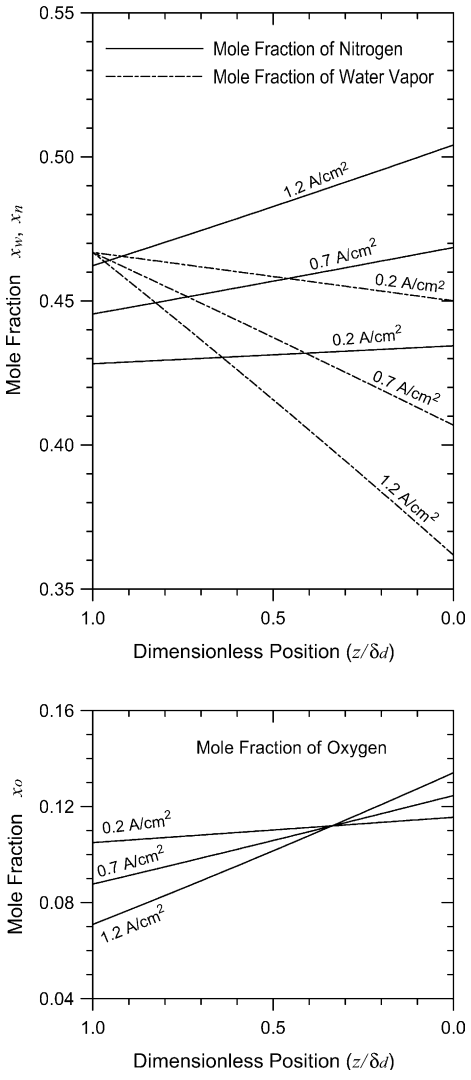

Fig. 3. Spatial variations of mole fraction within the one-dimensional GDL.

where $D_{\text{o-mix}}$ is the diffusivity of oxygen in the cathode gas mixture and C is the oxygen concentration. The first term on the right hand side of Eq. (10) is the oxygen molar flow rate resulting from the gas mixture bulk motion (convective transport). The second term denotes that resulting from the diffusion superimposed on the bulk flow (diffusive transport). The oxygen diffusivity, $D_{\text{o-mix}}$, in a multicomponent gas mixture with a bulk motion like that in the cathode is difficult to calculate [11,12], so we refer to the findings in Fig. 3 and the approach is discussed next.

From the linear variation in the oxygen concentration within the GDL, we may simplify the Eq. (10) expression by introducing an equivalent oxygen diffusivity, $D^{\text{e}}_{\text{o-mix}}$, and relating the oxygen molar flow rate to only its concentration gradient as:

$$N_{\text{o}} = -(\varepsilon^{3/2} D^{\text{e}}_{\text{o-mix}}) \frac{\Delta C}{\delta_{\text{d}}} \tag{11}$$

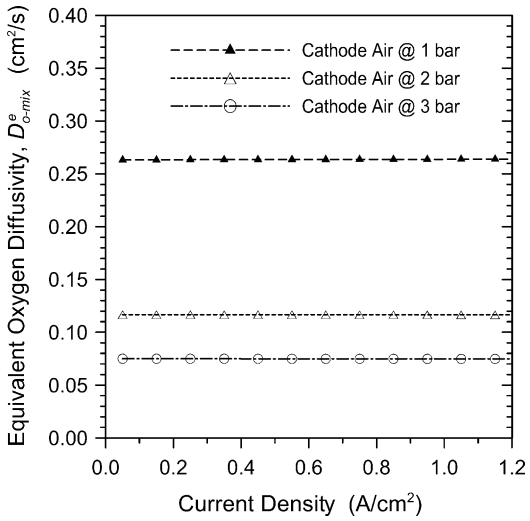

Fig. 4. Equivalent oxygen diffusivity in the cathode gas mixture.

where, $\Delta C = (x_{\text{o}}|_{z=\delta_{\text{d}}} - x_{\text{o}}|_{z=0}) P_t / RT$, is the drop in oxygen concentration across the GDL. The equivalent oxygen diffusivity in the cathode gas mixture can then be calculated from the relation between molar flow rate and oxygen concentration gradient.

Fig. 4 shows the $D^{\text{e}}_{\text{o-mix}}$ results calculated from the oxygen mole fraction profile for 1, 2 and 3 bar cathode air, respectively, as the current density varies from 0.05 to 1.2 A cm^{-2}. The equivalent oxygen diffusivities in the cathode gas mixture vary so slightly with the current density that they can be regarded as constant. The equivalent oxygen diffusivities were estimated as 0.263, 0.117 and 0.075, respectively, for 1, 2 and 3 bar cathode air.

3. Two-dimensional gas diffusion layer model

The two-dimensional model for the oxygen transport through the GDL takes the current collector ribs into account, as shown by the enlarged portion of the single cell appearing in Fig. 1. L_1 and L_2 denote the midline of the GDL portion in contact with the rib and the channel, respectively. A GDL element bounded by L_1, L_2 has been selected for analysis in this two-dimensional model.

3.1. Governing equation

The oxygen concentration along the catalyst layer is determined by that in the gas flow channel and by the mass transfer process within the GDL. The two-dimensional oxygen mass transport within the GDL can be described by rewriting Eq. (11) in vector form as:

$$\vec{N}_{\text{o}} = -(\varepsilon^{3/2} D^{\text{e}}_{\text{o-mix}}) \nabla C \tag{12}$$

where $\vec{N}_{\text{o}}$ is the oxygen molar flux (a vector quantity) in the GDL. By taking divergence of both sides of Eq. (12) and

by applying the species conservation for oxygen, we obtain the Laplace's equation that governs the oxygen concentration distribution within the GDL:

$$\nabla^2 C = \frac{\partial^2 C}{\partial y^2} + \frac{\partial^2 C}{\partial z^2} = 0 \tag{13}$$

3.2. Boundary conditions

The catalyst layer can be regarded as an infinitely thin film [1,13–15] located on the left boundary of the GDL. The rate of the electrochemical reaction within the catalyst layer can be described using this thin film model, yielding a Butler–Volmer rate expression. It is then simplified to give a Tafel type equation in terms of the oxygen concentration at the catalyst layer as:

$$i = A_v i_0 \delta_c \frac{C(y, \delta_d)}{C_{ref}} \exp\left(\frac{\alpha_c F \eta_c}{RT}\right) \tag{14}$$

In Eq. (14), i is the local current density, A_v the specific area of the active surface, i_0 the reference exchange current density, δ_c the thickness of the catalyst layer, $C(y, \delta_d)$ the oxygen concentration at the catalyst layer, C_{ref} the reference oxygen concentration associated with i_0, α_c the cathode transfer coefficient, and η_c the cathode overpotential.

In this two-dimensional model, both the local current density and the oxygen concentration at the catalyst layer vary with y. Furthermore, under the steady-state condition and the zero reactant crossover assumption, the current is determined by the oxygen diffusion rate at the GDL/catalyst layer interface. This indicates that:

$$\frac{i}{4F} = N_o|_{z=\delta_d} = -\varepsilon^{3/2} D^e_{o\text{-}mix} \left.\frac{\partial C}{\partial z}\right|_{z=\delta_d} \tag{15}$$

Combining Eq. (14) with Eq. (15), we obtain the following boundary condition for the GDL/catalyst layer interface:

$$\left.\frac{\partial C}{\partial z}\right|_{z=\delta_d} = -\frac{A_v i_0 \delta_c}{4F\varepsilon^{3/2} D^e_{o\text{-}mix}} \frac{C(y, \delta_d)}{C_{ref}} \exp\left(\frac{\alpha_c F \eta_c}{RT}\right) = -K \times C(y, \delta_d) \tag{16}$$

where the parameter K is defined as:

$$K = \frac{A_v i_0 \delta_c \exp(\alpha_c F \eta_c / RT)}{4F\varepsilon^{3/2} D^e_{o\text{-}mix} C_{ref}} \tag{17}$$

The K value can be evaluated for the given cathode overpotential η_c and the physical parameter and property values: A_v, i_0, δ_c, α_c, T, ε, $D^e_{o\text{-}mix}$ and C_{ref}.

It is appropriate to assume symmetrical boundary conditions on both the upper and lower boundaries of the GDL element; hence the condition $\partial C/\partial y = 0$ is imposed on both L_1 and L_2. The molar flow rate across the GDL/rib interface is zero, so the $\partial C/\partial z = 0$ condition applies to that part of the boundary. For simplicity, we set $C = C_0$ on the boundary facing the channel and assumed that the cathode overpotential η_c is constant along the catalyst layer.

The boundary conditions for the GDL element under study are summarized as:

$$\frac{\partial C}{\partial z} = -KC \quad \text{for } 0 \le y \le \frac{w_r + w_c}{2}, \text{ and } z = \delta_d \tag{18}$$

$$\frac{\partial C}{\partial y} = 0 \quad \text{for } y = \frac{w_r + w_c}{2}, \text{ and } 0 < z < \delta_d \tag{19}$$

$$\frac{\partial C}{\partial z} = 0 \quad \text{for } \frac{w_c}{2} \le y \le \frac{w_r + w_c}{2}, \text{ and } z = 0 \tag{20}$$

$$C = C_0 \quad \text{for } 0 \le y < \frac{w_c}{2}, \text{ and } z = 0 \tag{21}$$

$$\frac{\partial C}{\partial y} = 0 \quad \text{for } y = 0, \text{ and } 0 < z < \delta_d \tag{22}$$

3.3. Solution procedure

The two-dimensional Laplace's equation (Eq. (13)) associated with the corresponding boundary conditions (Eqs. (18)–(22)) has been discretized using the finite-difference approach and solved using an alternating-direction explicit (ADE) method [16]. From the solution, we obtain the oxygen concentration distribution in the GDL, i.e. $C(y,z)$. The oxygen molar flow rate at the GDL/catalyst layer interface, $N_o|_{z=\delta_d}$, and the local current density, i, are then evaluated using Eq. (15).

To indicate the performance of the partly-covered GDL in transporting oxygen from the gas flow channel to the catalyst layer, an assessment may be made by evaluating the effectiveness of the GDL, ξ_g. It is defined as the ratio of the mass transport rate through the GDL element (partly covered by the rib) to the mass transport rate obtained without the rib. Because the mass transport rate of oxygen is proportional to the current density, ξ_g can be expressed in terms of the current densities as:

$$\xi_g = \frac{I_{ave}}{I} \tag{23}$$

where I denotes the cell current density without ribs, and I_{ave} represents the average current density with ribs. This was evaluated using the following equation:

$$I_{ave} = \frac{1}{(w_r + w_c)/2} \int_0^{(w_r+w_c)/2} i(y)\mathrm{d}y \tag{24}$$

4. Results and discussion

4.1. Model validation

To validate the two-dimensional GDL model associated with the thin-film assumption for the catalyst layer, the fuel cell voltage is calculated and a comparison is made between the simulation results and experimental data.

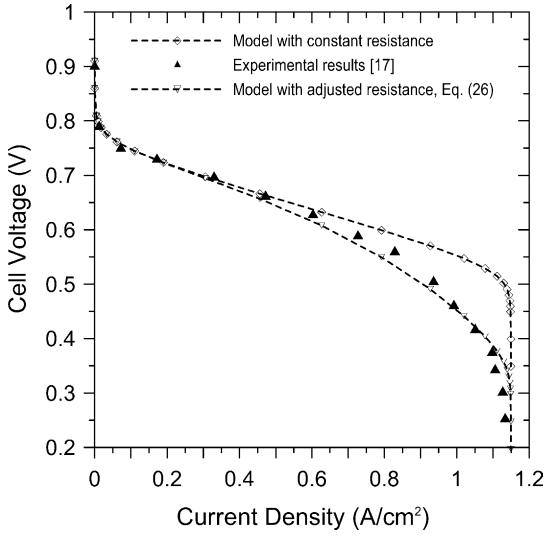

Fig. 5. Model fit for the two-dimensional model to the experimental data.

Neglecting the overpotential on the anode side, the fuel cell voltage is calculated as:

$$V_{\text{cell}} = V_{\text{oc}} - \eta_{\text{c}} - I_{\text{ave}}\Re \tag{25}$$

where V_{oc} is the open-circuit voltage and $\Re$ is the ohmic resistance through the fuel cell. Fig. 5 shows how our model fits with the experimental data, given by Springer et al. [17], for a PEM fuel cell with 0.3 mm GDL, 5 μm catalyst layer, and fed with H_2/air at 1 bar. The physical parameters and properties for the fit are listed in Table 2. A substantial discrepancy between the model fit with constant $\Re = 0.14\ \Omega\,\text{cm}^2$ and the experimental data has been found at higher current densities. For the limiting current density, however, a good match can be seen between the model fit and the experimental data. The discrepancy at higher current densities can be attributed to the increased ohmic resistance of the drying membrane when the fuel cell is operating at high current densities, or to the ohmic resistance arising in the catalyst layer that has been neglected in the thin-film model. Accounting for these effects, we have adjusted the ohmic resistance value with the increase in current density using the following relation:

$$\Re = 0.14 + 0.1(I_{\text{ave}})^2 \tag{26}$$

As can be seen from Fig. 5, a good agreement has been achieved for the operating range up to the limiting current density of 1.15 A cm^{-2}.

Table 2
Physical parameter and property values used in two-dimensional model

Physical parameter/property	Value
Cell temperature, T (K)	353.15
Cathode transfer coefficient, α_{c}	2.0
Thickness of catalyst layer, δ_{c} (μm)	5.0
Thickness of gas diffusion layer, δ_{d} (cm)	0.03
Width of current collector rib, w_{r} (cm)	0.15
Width of gas flow channel, w_{c} (cm)	0.15
Reference exchange current density times area, $A_v i_0$ (A cm^{-3})	5×10^{-4}
Reference oxygen concentration, C_{ref} (mol cm^{-3})	4.62×10^{-6}
Oxygen concentration at GDL/channel interface, C_0 (mol cm^{-3})	4.62×10^{-6}
Porosity of gas diffusion layer, ε	0.25
Cathode pressure, P_t (bar)	1.0
Equivalent oxygen diffusivity, $D^{\text{e}}_{\text{o-mix}}$ (cm^2 s^{-1})	0.263
Nitrogen–oxygen mole ratio in gas flow channel	3.76
Ohmic resistance, $\Re$ (Ω cm^2)	0.14

4.2. Concentration distribution and current density variation

The oxygen concentration distribution within the GDL element accompanied by the variation in local current density i along the catalyst layer is shown in Fig. 6 for three average current densities. The same parameters listed in Table 2 were used for the simulations.

For the average current density of 0.1 A cm^{-2}, minor variations in the oxygen concentration (ranging from 0.78 C_0 to C_0) and local current density i along the catalyst layer (ranging from 0.087 to 0.107 A cm^{-2}) have been observed. Mathematical reasoning has suggested that the local current density i at y = 0 be identical to the current density for the PEM fuel cell without current collector ribs and hence ξ_{g} has been found to be as high as 93%.

Fig. 6(b) gives the results for the average current density of 0.5 A cm^{-2}. Because of the increase in average current density, a higher concentration gradient is required to transport more oxygen to the catalyst layer. A substantial variation in oxygen concentration has been found (ranging from 0.2 C_0 to C_0). The local current density for the portion covered by the rib is substantially lower than that facing the channel. The local current density ranges from 0.22 to 0.71 A cm^{-2} and ξ_{g} drops to 70%.

As the average current density increases further to 1.0 A cm^{-2}, from Fig. 6(c) the oxygen concentration can be seen to have varied drastically and only a trace of oxygen can be found in the inner portion covered by the rib. At the catalyst layer for $y \geq w_{\text{c}}/2$, the local current density i decreases from 1.2 to 0.11 A cm^{-2}, which is only about 1/15 of the current density at y = 0, and ξ_{g} is as low as 60%. This phenomenon can be attributed to the GDL being so thin (δ_{d} = 0.3 mm), as compared to the rib width (w_{r} = 1.5 mm), that the small cross-sectional area of the path restricts the mass transfer from the gas flow channel to the $y > w_{\text{c}}/2$ portion, especially when the total mass transfer rate is high.

The results shown in Fig. 6 are based on the assumption that the cathode overpotential η_{c} is constant along the catalyst layer. But when the ohmic voltage drop across the membrane is taken into account, the non-uniformity in the current density might be mitigated.

4.3. Influence of w_r and w_c on GDL effectiveness

To investigate the rib and channel size effects on the oxygen mass transport through the GDL, a series of model simulations has been conducted to evaluate the GDL effectiveness with the rib and channel widths being varied while all of the other parameters remained the same as listed in Table 2.

Fig. 7 shows the variation in ξ_g versus the cell current density for nine sets of w_r and w_c combinations. The circles at the end of each curve indicate that the limiting current conditions were reached for the given w_r and w_c combination. No more data points are expected to appear further right. It is obvious that ξ_g decreases with the rib width and increases with the channel width. All of the ξ_g curves fall with the current density, indicating that the GDL is utilized less effectively at higher current densities. Because the GDL portion covered by the rib can still be utilized to a certain extent even at high current densities, the ξ_g value at the limiting current density is slightly higher than the channel width fraction $w_c/(w_r + w_c)$.

4.4. GDL thickness effects on cell performance

For the rib-covered GDL portion ($y > w_c/2$), faster mass transport can be achieved by increasing the GDL thickness because it will enlarge the path for oxygen transport in the y-direction. However, as for the channel-facing portion ($y < w_c/2$), the oxygen mass transport rate decreases with the increase in GDL thickness. Thus, there may exist an optimal

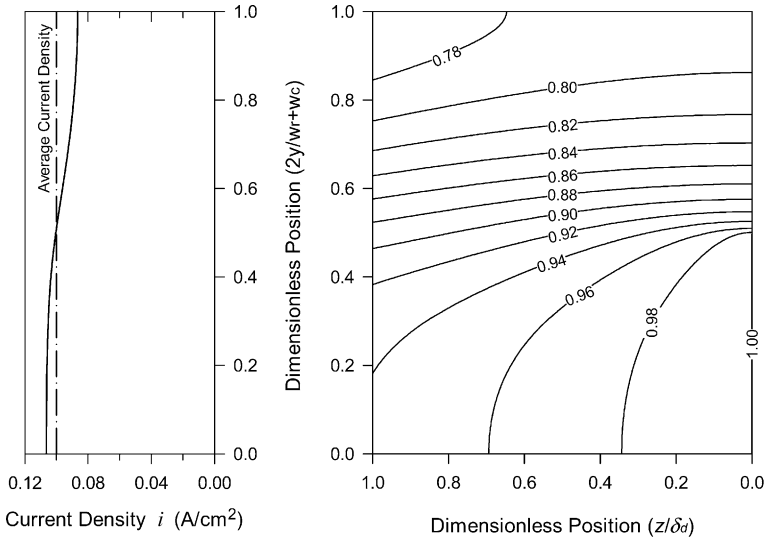

(a) $I_{ave} = 0.1$ A/cm^2

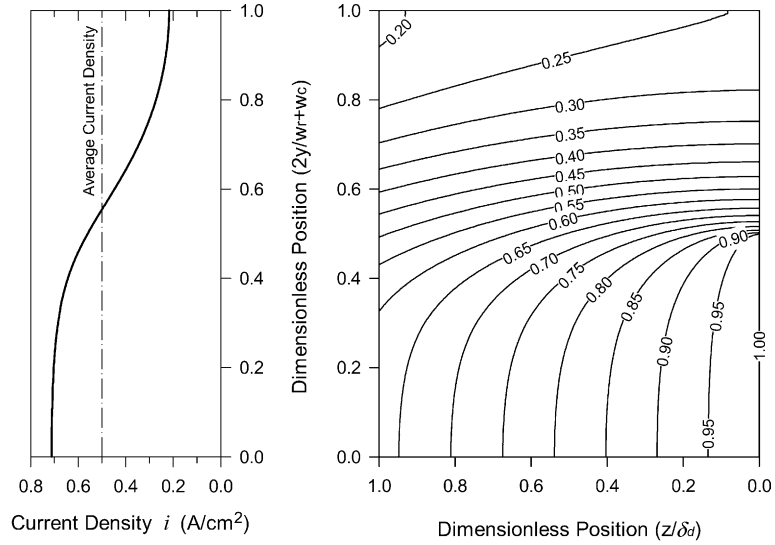

(b) $I_{ave} = 0.5$ A/cm^2

Fig. 6. Distribution of oxygen concentration within the GDL element and the variation in local current density along the catalyst layer (the numerical labels on the iso-concentration curves designate their C/C_0 values).

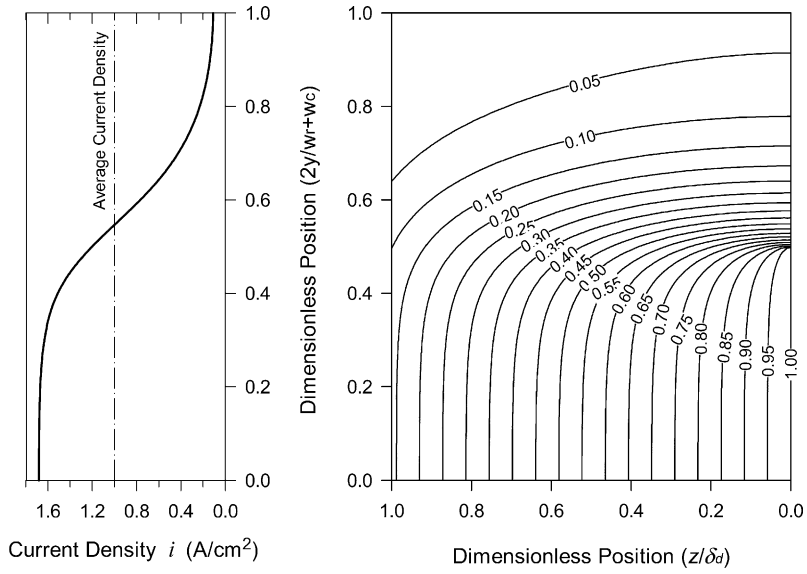

(c) I_{ave} = 1.0 A/cm^2

Fig. 6. (*Continued*).

thickness for the GDL under a given set of w_r and w_c, and this possibility will be further explored below.

Fig. 8 shows the calculated performance curves for a single PEM fuel cell of various GDL thicknesses with all of the other parameters being identical to those listed in Table 2. As can be seen, the overall performance falls with the increase in GDL thickness. A very slight discrepancy in cell voltage occurs at low current densities, but substantial deviation appears at mid and high current densities. The limiting current density decreases as the thickness increases.

The current density at V_{cell} = 0.6 V (a typical operating voltage of PEM fuel cells) has been singled out for quantitative investigations. The current density versus GDL thickness is plotted in the inset in Fig. 8 together with the other two sets of w_r and w_c. The relationship among the three curves in the inset reflects their relative ranking in terms of ξ_g, as depicted in Fig. 7. The curves in the inset fall with the increase of GDL thickness and no optimal thickness for the GDL has been found.

We should bear in mind that, in addition to thickness, the porosity of the GDL also influences the effective cross-sectional area of the oxygen transport path in the *y*-direction. Fig. 9 shows the cell's current density (again at V_{cell} = 0.6 V) versus GDL thickness of various GDL porosities, with both

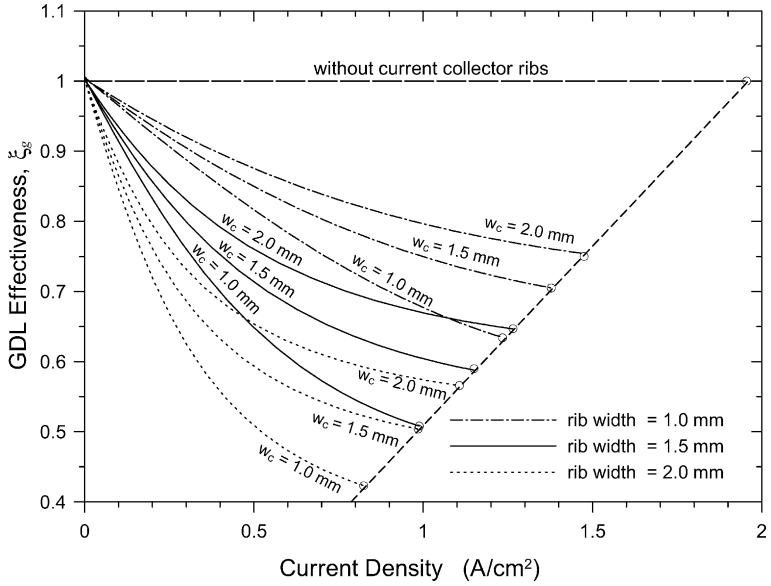

Fig. 7. GDL effectiveness vs. current density for various rib and channel widths.

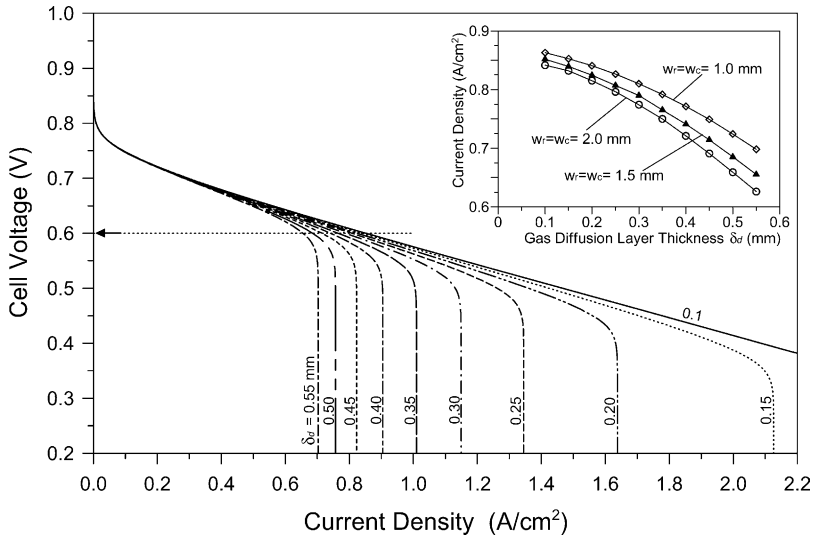

Fig. 8. Calculated performance curves for a single PEM fuel cell at various GDL thicknesses.

the rib and the channel measured 1.5 mm in width. It can be seen from the curves that the performance of a PEM fuel cell has substantially enhanced with an increase in the GDL porosity. As the porosity increases to 0.5 or above, a maximum current density emerges and the maxima are designated on each curve by circles. The curves in Fig. 9 indicate that, from the mass transfer point of view, the GDL thickness should be as thin as possible if the GDL porosity is low. However, an optimal GDL thickness exists when a high-porosity GDL is used.

For electrical conductivity, material strength and ease of fabrication considerations, the GDL generally has a porosity substantially lower than 1.0. Under such a design restriction, an increase of the oxygen mass transport in the *y*-direction may offer the possibility of enhancing the overall effectiveness of the GDL. This may be carried out by using a GDL that has a directional preference in transporting oxygen. For instance, yarns of carbon cloth parallel to the channel flow direction are substantially thinner than that of perpendicular yarns, and a sparser arrangement can be made for yarns to be perpendicular to the channel flow.

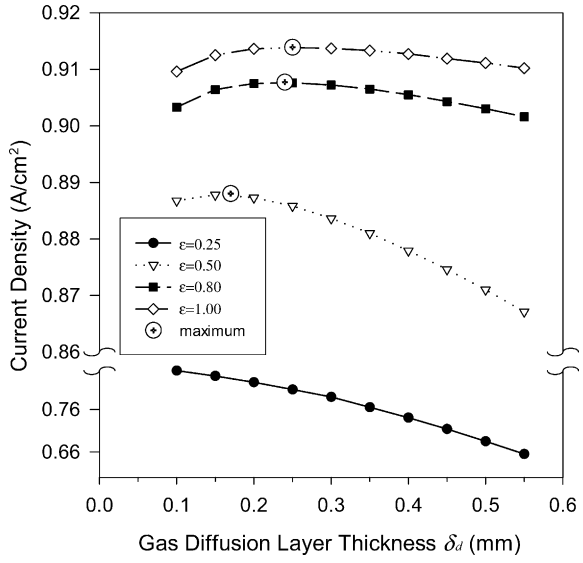

Fig. 9. Cell current density (at 0.6 V) vs. GDL thickness for various GDL porosities.

5. Conclusions

We have developed a two-dimensional model that simplifies the descriptions of kinetic and mass transfer processes in PEM fuel cell cathode. This model is validated with experimental data from the literature and is used to investigate the mass transfer problem within the GDL under the influence of current collector ribs.

The GDL can be used effectively at low current densities; however, its effectiveness falls with increasing current density. At high current densities, the effectiveness of the GDL is only slightly higher than the channel width fraction $w_c/(w_r + w_c)$. The mass transfer is slow in the GDL portion covered by the ribs and only a trace of oxygen can be found in the inner part when the current density is high.

From the mass transfer point of view, the GDL thickness should be as thin as possible if the GDL porosity is low. However, an optimal thickness for the GDL exists when a high-porosity GDL is used. The existence of such an optimal GDL thickness implies that a GDL with directional preference in mass transfer can be used to improve PEM fuel cell performance.

References

[1] A.C. West, T.F. Fuller, J. Appl. Electrochem. 26 (1996) 557.
[2] P.L. Hental, J.B. Lakeman, G.O. Mepsted, P.L. Adcock, J. Power Sources 80 (1999) 235.

[3] W.M. Yan, C.Y. Soong, F.L. Chen, H.S. Chu, J. Power Sources 125 (2004) 27.
[4] C.W. Tobias, Advances in Electrochemistry and Electrochemical Engineering, John Wiley, New York, 1962.
[5] T.E. Springer, T.A. Zawodzinski, S. Gottesfeld, J. Electrochem. Soc. 138 (8) (1991) 2334.
[6] T. Okada, G. Xie, M. Meeg, Electrochim. Acta 43 (14–15) (1998) 2141.
[7] K.H. Choi, D.H. Peck, C.S. Kim, D.R. Shin, J. Power Sources 86 (2000) 197.
[8] G.J.M. Janssen, M.L.J. Overvelde, J. Power Sources 101 (2001) 117.
[9] K.T. Jeng, C.W. Chen, J. Power Sources 112 (2002) 367.
[10] D.M. Bernardi, M.W. Verbrugge, AIChE J. 37 (8) (1991) 1151.
[11] Chemical Engineers Handbook, fifth ed., McGraw-Hill, New York, 1973.
[12] R.B. Bird, W.E. Stewart, E.N. Lightfoot, Transport Phenomena, John Wiley, New York, 1960.
[13] Y. Butel, P. Ozil, R. Durand, Electrochim. Acta 43 (9) (1998) 1077.
[14] Z.H. Wang, C.Y. Wang, K.S. Chen, J. Power Sources 94 (2001) 40.
[15] M.S. Wilson, S. Gottessfeld, J. Appl. Electrochem. 22 (1992) 1.
[16] D.A. Anderson, J.C. Tannehill, R.H. Pletcher, Computational Fluid Mechanics and Heat Transfer, McGraw-Hill, New York, 1984.
[17] T.E. Springer, M.S. Wilson, S. Gottesfeld, J. Electrochem. Soc. 140 (12) (1993) 3513.